Available online at www.sciencedirect.com
SCIENCE DIRECT®
Journal of Organometallic Chemistry 689 (2004) 3481–3491
Journal of Organometallic Chemistry
www.elsevier.com/locate/jorganchem

Preference of di-*n*-butyltin^{IV} compounds to build O···Sn bonds in fused rings with five-six members

Norberto Farfán [a,*], Teresa Mancilla [a], Rosa Santillan [a], Atilano Gutiérrez [b], Luis S. Zamudio-Rivera [c], Hiram I. Beltrán [c,*]

[a] *Departamento de Química, Centro de Investigación y de Estudios, Avanzados del Instituto Politécnico Nacional, Apdo, Postal 14-740, 07000 México, DF México*

[b] *Laboratorio de Resonancia Magnética Nuclear, Universidad Autónoma Metropolitana, San Rafael Atlixco 186 Col. Vicentina, Unidad Iztapalapa, 09340, DF, México*

[c] *Programa de Ingeniería Molecular, Instituto Mexicano del Petróleo, Eje Central Lázaro Cárdenas No. 152, Apartado Postal 14-805, 07730 México*

Received 5 May 2004; accepted 20 July 2004
Available online 11 September 2004

Abstract

The reaction of salicylaldehyde (**1**), *o*-aminophenols (**2a**–**2f**), and di-*n*-butyltin^{IV} oxide (**3**) to give six di-*n*-butyltin^{IV} compounds (**4a**–**4f**) was achieved in good yields. All compounds were characterized by ^{1}H, ^{13}C, ^{15}N, ^{119}Sn NMR, mass spectrometry, IR, elemental analysis and in the case of compounds **4a**, **4b**, **4d** and **4e** by X-ray diffraction analysis. Compound **4a** crystallized with trigonal bipiramidal (TPB) geometry surrounding the tin atom while **4b** and **4e** crystallized as dimeric molecules joined by two O···Sn bonds with distorted octahedron (DOC) geometry. The X-ray structure of **4d** presents one cocrystallized monomeric TBP with one dimeric DOC molecule. Correlations of $\sigma_{Hammett}$ vs. spectroscopic values were found for **4a**–**4b** and **4d**–**4f**, indicating the substituents in the aromatic ring derived from *o*-aminophenol serve as modulators of the O···Sn supramolecular interaction. The O···Sn bond formation is selective for the five-membered ring oxygen atom.

Keywords: Di-*n*-butyltin^{IV}; Multinuclear NMR; X-ray structures; Sigma Hammett; Schiff base

1. Introduction

Since Pedersen, Lehn and Cram were awarded the Nobel Prize in 1987 "*for their development and use of molecules with structure-specific interactions of high selectivity*" [1], many scientific as well as technological aspects have been approached within the realm of Supramolecular Chemistry [2–6]. Our recent work in tin chemistry is directed to the X–Sn···Y bond formation (where X and Y are mainly N or O), this bond has the ability to build supramolecular aggregates of trimeric, hexameric, oligomeric and polymeric states [7–10]. Therefore, elucidation of the supramolecular bonding of molecules containing tin should provide basis to understand the recognition processes with natural receptors and explain their activities as anticancer agents and towards bacteria [11,12].

A crystallographic search of the CCDC data base [13] reveals that tin^{IV} compounds with di-*n*-butyl and diphenyl substituents constructed from rigid tridentate ligands, result in formation of monomeric species, both in solution and in the solid-state [14–17]. Reported X-ray structures of dimeric tin^{IV} compounds are scarce and refer mainly to bidentate ligands containing 6:4:6 fused rings (Scheme 1) [14,18–23]. The use of tridentate

* Corresponding authors.
E-mail addresses: jfarfan@mail.cinvestav.mx (N. Farfán), hbeltran@www.imp.mx (H.I. Beltrán).

0022-328X/$ - see front matter © 2004 Elsevier B.V. All rights reserved.
doi:10.1016/j.jorganchem.2004.07.053

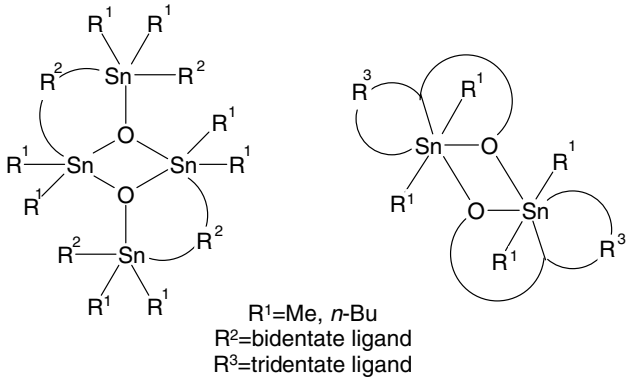

Scheme 1. Dimeric tin^{IV} compunds with Sn_2O_2 core.

ligands which have oxygen, nitrogen and sulfur as donor atoms promotes formation of X → Sn (X = N, O, S) bonds with a Sn_2X_2 core (X = S, O) that lead to dimeric molecules with five–five and six–six fused rings [23–26] (Scheme 1).

It is worth mentioning that di-organotin^{IV} compounds containing rigid tridentate ligands have shown quadratic nonlinear optical response [27]. This response is attributed to push–pull modulation through the tin atom and hence this type of compounds could serve as second harmonic generation prototypes. The latter work [27] represents the only example of dimeric diorganotin derivatives with rigid tridentate ligands, where the preference of the Sn_2O_2 ring formation is selective for the five-membered ring oxygen atom.

Herein, we present six molecular candidates possessing fused five: six-membered rings, specially designed to show the preference for O···Sn bond formation when two different Sn–O groups are present; since we are interested in exploring the chemistry and coordinating behavior of di-*n*-butyltin^{IV} compounds in the solid state and in solution.

2. Results and discussion

2.1. One pot method

The method involves equimolecular addition of salicylaldehyde (**1**), *ortho*-aminophenol (**2a**–**2f**) and di-*n*-butyltin^{IV} oxide (**3**) to a 4:1 benzene/ethanol mixture maintained at reflux for 8 h to give the products **4a**–**4f** in 74–96% yield (Scheme 2). Compound **4a** has been previously synthesized through a two step procedure, and characterized by ^{1}H NMR, IR and elemental analysis [28]. In addition, we describe herein the complete structural characterization by ^{1}H, ^{13}C, ^{15}N, ^{119}Sn, MAS-high power NMR, IR, mass spectrometry, elemental analysis and single crystal X-ray structure.

2.2. Solution NMR

The ^{1}H NMR (Table 1) spectra shows a single signal for H-7 between 8.79 and 8.58 ppm. For all compounds the *n*-butyl signals are isochronous, evidencing that there is no fluxional or asymmetric behavior. In general the following order is observed for these signals: H-β from 1.64 to 1.61 ppm, H-α from 1.53 to 1.48 ppm, H-γ from 1.33 to 1.30 ppm, while H-δ appears from 0.86 to 0.83 ppm.

The signal for C-9 (170.9 and 169.4 ppm), in the ^{13}C NMR spectra (Table 2), is shifted to high frequency due to the polarization of the C=N bond. The *n*-butyl signals are isochronous showing the C-β between 27.2 and 26.9 ppm, C-γ from 26.8 to 26.6 ppm, C-α from 22.6 to 22.0 ppm and finally C-δ from 13.8 to 13.6 ppm.

The ^{15}N signals for compounds **4a**–**4f** (−175.7 and −166.2 ppm, Table 3), are shifted 100 ppm to lower frequencies compared with non-coordinated imines [29]. These chemical shifts evidence the increase in coordina-

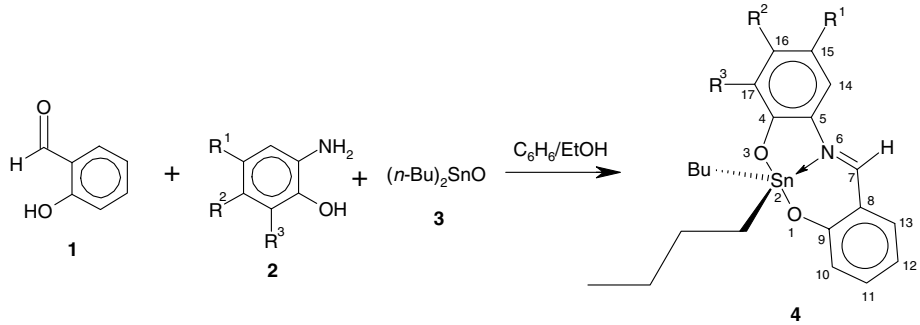

	R1	R2	R3
a	H[18]	H	H
b	Me[18]	H	H
c	Me[18]	H	Me[19]
d	Cl	H	H
e	NO_2	H	H
f	H	NO_2	H

Scheme 2. Numbering and preparation of compunds **4a**–**4f**.

Table 1
^{1}H NMR data of 2,2-di-*n*-butyl-6-aza-1,3-dioxa-2-stanna-[d,h] dibenzocyclononenes **4a**–**4f** in $CDCl_3$

Compound	H-7	H-10	H-11	H-12	H-13	H-14	H-15	H-16	H-17	H-α	H-β	H-γ	H-δ
4a	8.65	6.81, d	7.39, ddd, J_0 = 8.4	6.74, dd	7.25, dd, J_0	7.34, dd, J_0 = 8.0	6.69, ddd, J_0 = 8.0	7.18, ddd, J_0 = 8.4	6.86, dd, J_0 = 8.4	1.50	1.64	1.33, sx	0.85, t
	s	J_0 = 8.4	7.0, J_m = 1.5	J_0 = 8.0, 7.0	J_m = 1.5	J_m = 1.1	7.5, J_m = 0.9	7.5, J_m = 1.1	J_m = 0.9	m	m	J = 7.3	J = 7.3
4b	8.70	6.80, dd, J_0 = 8.8	7.38, ddd, J_0 = 8.8	6.74, ddd, J_0 = 8.8	7.26, ddd, J_0 = 8.1	7.15, d	–	7.00, dd, J_0 = 8.4	6.77, d	1.48	1.63	1.32, sx	0.84, t
	s	J_0 = 1.1	8.1, J_m = 1.8	8.1, J_m = 1.1	J_m = 1.8	J_m = 1.7	–	J_m = 1.7	J_0 = 8.4	m	m	J = 7.3	J = 7.3
4c	8.62	6.81, d	7.37, ddd, J_0 = 8.6	6.72, dd	7.24, dd, J_0 = 7.9	7.02	–	6.92	–	1.49	1.62	1.33, sx	0.86, t
	s	J_0 = 8.6	6.9, J_m = 1.2	J_0 = 7.9, 6.9	J_m = 1.2	s	–	s	–	m	m	J = 7.3	J = 7.3
4d	8.58	6.80, d	7.41, dd	6.75, dd	7.26, d	7.31, d	–	7.11, dd, J_0 = 8.8	6.77, d	1.49	1.69	1.32, sx	0.85, t
	s	J_0 = 8.4	J_0 = 8.4, 7.3	J_0 = 7.7, 7.3	J_0 = 8.1	J_m = 2.2	–	J_m = 2.2	J_0 = 8.8	m	m	J = 7.3	J = 7.3
4e	8.79	6.78, d	7.34, ddd, J_0 = 8.2	6.77, dd	7.34, dd, J_0 = 8.0	8.33, d	–	8.08, dd, J_0 = 8.2	6.78, d	1.53	1.63	1.30, sx	0.83, t
	s	J_0 = 8.2	6.7, J_m = 1.7	J_0 = 8.0, 6.7	J_m = 1.7	J_m = 2.7	–	J_m = 2.7	J_0 = 8.2	m	m	J = 7.3	J = 7.3
4f	8.71	6.79, d	7.44, ddd, J_0 = 8.7	6.75, dd	7.28, dd, J_0 = 7.9	7.38, d	7.53, dd, J_0 = 8.6		7.61, d	1.52	1.61	1.31, sx	0.83, t
	s	J_0 = 7.7	7.7, J_m = 1.8	J_0 = 8.7, 7.9	J_m = 1.8	J_0 = 8.6	J_m = 2.5	–	J_m = 2.5	m	m	J = 7.3	J = 7.3

4b: 2.32, s, H-18. **4c**: 2.30, bs, H-18; 2.23, bs, H-19.

Table 2
^{13}C NMR data of 2,2-di-*n*-butyl-6-aza-l,3-dioxa-2-stanna-[d,h]dibenzocyclononenes **4a**–**4f** in $CDCl_3$

Compound	C-4	C-5	C-7	C-8	C-9	C-10	C-ll	C-12	C-13	C-14	C-15	C-16	C-17	C-α	C-β	C-γ	C-δ
4a	159.6	131.7	161.7	117.9	169.6	122.5	136.7	116.9	135.2	114.8	116.3	130.1	118.6	22.0	27.0	26.6	13.6
4b	157.5	131.2	161.5	118.1	169.6	122.6	136.7	117.0	135.3	115.2	125.7	131.1	118.4	22.1	27.2	26.8	13.8
4c	156.2	130.3	161.1	118.2	169.4	122.5	136.3	116.8	135.1	112.5	124.6	131.6	127.5	22.0	27.2	26.7	13.7
4d	158.2	132.2	162.3	117.8	169.9	122.6	137.2	117.1	135.4	115.0	120.7	129.7	119.4	22.2	27.0	26.6	13.6
4e	166.0	131.5	164.3	117.8	170.3	122.7	138.3	117.7	136.1	111.9	137.2	126.0	117.9	22.6	26.9	26.6	13.6
4f	159.7	137.5	164.7	117.7	170.9	123.0	138.4	117.6	135.9	115.0	111.3	148.5	113.1	22.5	27.0	26.7	13.6

4a: 21.0, C-18. **4c**: 21.0, C-18; 16.6, C-19.

tion number of nitrogen and confirm the formation of the N → Sn bond [7,27].

The ^{119}Sn NMR measurements summarized in Table 3 were obtained in non-coordinating ($CDCl_3$) and coordinating (DMSO-d_6) solvents. The ^{119}Sn chemical shifts are in the range from −185.1 to −175.1 ppm in $CDCl_3$, characteristic for pentacoordinated tin atoms and they shift from −213.4 to −211.6 ppm in DMSO-d_6, due to coordination of the oxygen atom from the solvent to tin. Thus the change in chemical shift for the tin signal directly reflects an increase in the coordination number, as in the case of the ^{15}N signals.

The $|^1J(^{119}Sn–^{13}C)|$ coupling constants summarized in Table 3 show values between 619.9 and 608.3 Hz, characteristic for distorted TBP tin atoms in $CDCl_3$ solution while the $|^3J(^{119}Sn–^1H7)|$ coupling constants are between 46.7 and 42.3 Hz.

2.3. Solid-state NMR

For compounds **4a** and **4b** the ^{119}Sn MAS-high power decoupled NMR spectra were recorded. The chemical shifts for the powder samples are −185.8 ppm for **4a** (−185.1 ppm for **4a**, in $CDCl_3$) and −220.2 ppm for **4b** (the chemical shift in $CDCl_3$ solution is −183.7 and −211.6 ppm in DMSO-d_6). It is noteworthy that one can determine the coordination number of tin by measuring the solid NMR spectra, in analogy to solution measurements. The molecular preference to increase/decrease the coordination number in powder samples is mainly modulated by electronic factors as evidenced by the comparison of the solid and liquid NMR data, the X-ray structures of **4a** and **4b**, and into a lesser extent by the reaction conditions and the method used to isolate the powder sample.

2.4. X-ray structures

Compounds **4a**, **4b**, **4d** and **4e** were successfully crystallized and their structures determined by single crystal X-ray diffraction analysis (Figs. 1 and 2 show examples for penta- and hexa-coordinated structures containing

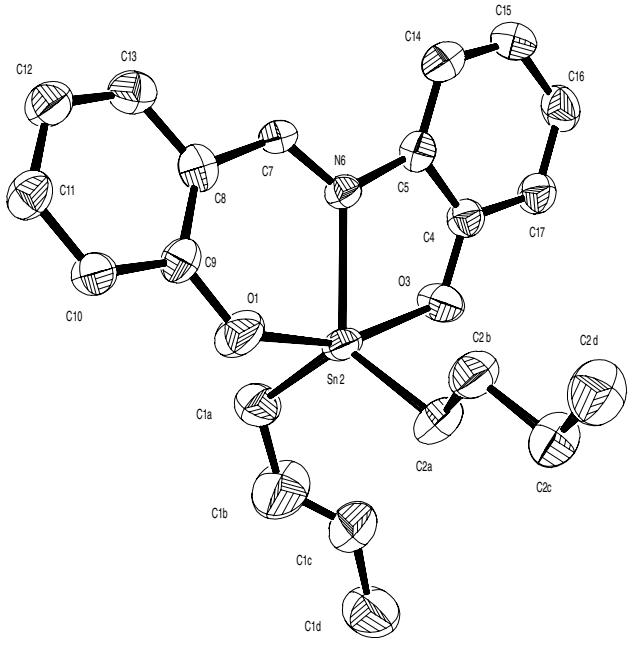

Fig. 1. TBP molecular structures for **4a** and **4d**.

Table 3
^{15}N and ^{119}Sn NMR data and coupling constants for 2,2-di-*n*-bntyl-6-aza-1,3-dioxa-2-stanna-[d,h]dibenzocyclononenes **4a–f**

Compound	δ ^{15}N	^{119}Sn($CDCl_3$)	δ ^{119}Sn(DMSO-d_6)	$J(^{119/117}$ Sn-^{13}C-α)	$^3J(^{119}$Sn-^{1}H7)
4a	−169.0	−185.1	−213.4	619.6/591.9	46.5
4b	−168.4	−183.7	−211.6	619.9/592.5	46.5
4c	−166.2	−183.0	[a]	619.2/592.0	46.7
4d	−171.5	−180.1	−218.5	616.5/588.9	44.0
4e	−177.3	−175.1	−240.8	608.3/583.4	43.3
4f	−175.7	−175.3	−231.6	610.4/581.3	42.3

[a] Insoluble in DMSO-d_6.

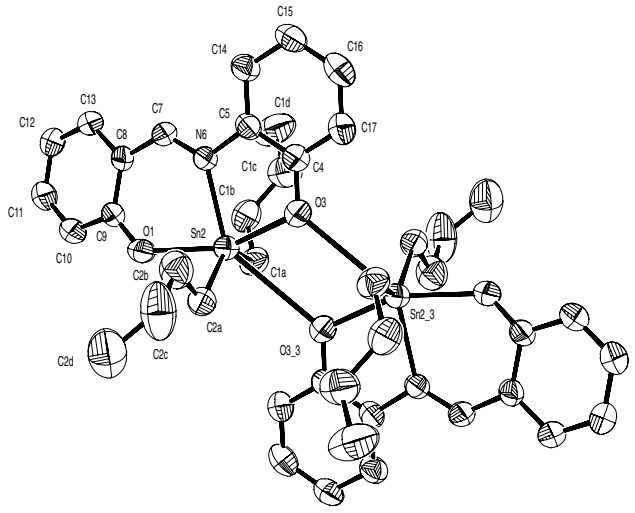

Fig. 2. DOC molecular structures for **4b**, **4d** and **4e** (n-butyl substituents were omitted for clarity).

tin). Details of data collection are given in Table 4, selected geometrical parameters are shown in Table 5.

Compound **4a** crystallized with a distorted TBP geometry around the tin atom, with the two oxygen atoms placed in axial positions. The two *n*-butyl groups and the nitrogen are placed in the equatorial plane. Compound **4d** crystallized with three molecules in the asymmetric unit, one of them retained a distorted TBP shape surrounding the tin atom, the other two exhibit a dimeric assembly through intermolecular O(3)···Sn(2) bridges of 2.830(4) and 2.899(4) Å in magnitude. Compounds **4b** and **4e** present dimeric assemblies where the O(3)···Sn(2) bridges have magnitudes of 3.0553(24) Å for **4b** and 3.2064(21) Å for **4e**. These values are shorter than the sum of the van der Waals radii (2.17 Å for tin and 1.52 Å for oxygen) [30]. Additionally, the Sn–O···Sn–O torsion angles evidence coplanarity since there is a 1° deviation for all dimeric molecules. The dimeric assembly occurs via Sn_2O_2 four-membered ring formation and constitutes one of the first examples of dimerization of a rigid tridentate ligand through Sn_2O_2 core formation [27]. The O···Sn bonding is formed with the oxygen atom in the five-membered ring and can be attributed to the increased "s" character at the five-membered ring.

The N(6) → Sn(2) bond distances are 2.205(6) Å for **4a**, 2.220(3) Å for **4b**, 2.224(4), 2.223(4) and 2.198(4) Å for the three molecules in **4d**, 2.213(2) Å for **4e**, these values are longer than those reported in the literature for di-*n*-butyltin^{IV} (2.180 Å) compounds (in dichloride tin derivatives the N–Sn distance is shorter, 2.166(8) Å because the tin atom is more acidic) [16,24]. The Sn(2)–O(1) bond distances are 2.082(4) Å for **4a**, 2.165(2) Å for compound **4b**, 2.146(4), 2.151(4) and 2.082(5) Å for the three molecules in **4d**, 2.150(2) Å for **4e**, showing values similar to carboxylic compounds previously reported (2.139 Å) [7,8,16,24]. The Sn(2)–O(3) distances are 2.119(4) Å for compound **4a**, 2.095(2) Å for **4b**, 2.110(3), 2.108(3) and 2.104(4) Å for the three molecules present in **4d**, 2.129(2) Å for **4e**, these are slightly longer

Table 4
Collection data and refinement parameters for Compounds **4a**, **4b**, **4d** and **4e**

Compound	**4a**	**4b**	**4d**	**4e**
Molecular formula	$C_{21}H_{27}NO_2Sn$	$C_{22}H_{29}NO_2Sn$	$C_{63}H_{72}Cl_3N_3O_6Sn_3$	C_{24} $H_{23}NO_3Sn$
Molecular weight	444.13	458.15	1429.66	489.13
Crystalline system	Monoclinic	Monoclinic	Triclinic	Monoclinic
Space group	$P2_1/n$	$P2_1/c$	$P\bar{1}$	$P2_1/c$
Unit cell dimensions				
a (Å)	8.9213(12)	9.3445(10)	12.542(9)	9.4438(2)
b (Å)	19.9510(13)	18.5938(10)	13.504(5)	18.4600(4)
c (Å)	11.6428(16)	12.0119(10)	20.558(5)	11.9803(3)
α (°)	90	90	93.70(3)	90
β (°)	101.953(13)	93.156(8)	105.50(4)	91.943(2)
γ (°)	90	90	104.85(5)	90
Volume (Å^3)	2027.4(4)	2083.9(3)	3210.0(30)	2087.36(8)
Z	4	4	6	4
ρ (mg/m^3)	1.455	1.460	1.479	1.556
μ (mm^{-1})	1.273	1.241	1.333	1.253
θ range (°)	2.55 to 25.99	2.18 to 24.97	2.38 to 26.29	3.49 to 27.48
Collected reflections	4256	4131	13614	7625
Independent reflections (R_{int})	3962 (0.0603)	3641 (0.0221)	12994 (0.0212)	4646 (0.0298)
θ completeness (%)	25.99° (99.8)	24.97° (99.8)	26.29° (99.7)	27.48° (97.0)
Data/restrictions/parameters	3962/21/277	3641/0/299	12994/154/838	4646/60/344
Goodness-of-fit on F^2	1.081	1.075	1.074	1.037
Final indices [$I > \sigma(I)$]	$R_1 = 0.0376$, $wR_2 = 0.1036$	$R_1 = 0.0360$, $wR_2 = 0.0977$	$R_1 = 0.0406$ $wR_2 = 0.1063$	$R_1 = 0.0327$, $wR_2 = 0.0802$
Final indices (all data)	$R_1 = 0.0607$, $wR_2 = 0.1201$	$R_1 = 0.0471$, $wR_2 = 0.1048$	$R_1 = 0.0769$, $wR_2 = 0.1279$	$R_1 = 0.0428$, $wR_2 = 0.0872$
$\Delta\rho_{min}$ (e/Å^3)	−0.856	−0.950	−0.751	−0.530
$\Delta\rho_{max}$ (e/Å^3)	0.789	0.892	0.826	0.565

Table 5
Collection data and refinement parameters for compounds **4a**–**4e**

Compound	**4a**	**4b**	**4d**			**4e**
			Mol. 1	Mol. 2	Mol. 3	
Bond distances (Å)						
N(6)–Sn(2)	2.205(6)	2.220(3)	2.224(4)	2.223(4)	2.198(4)	2.213(2)
C–Sn(2)	2.138(6)	2.131(4)	2.113(6)	2.132(6)	2.127(8)	2.123(3)
C–Sn(2)	2.093(5)	2.122(4)	2.118(6)	2.127(6)	2.109(9)	2.129(3)
O(1)–Sn(2)	2.082(4)	2.165(2)	2.146(4)	2.151(4)	2.082(5)	2.150(2)
O(3)–Sn(2)	2.119(4)	2.095(2)	2.110(3)	2.108(3)	2.104(4)	2.129(2)
N(6)–C(7)	1.295(8)	1.293(4)	1.296(6)	1.287(6)	1.304(6)	1.299(4)
C(9)–O(1)	1.315(5)	1.317(4)	1.300(6)	1.305(6)	1.310(7)	1.311(4)
C(4)–O(3)	1.326(6)	1.338(4)	1.327(6)	1.321(6)	1.320(6)	1.315(4)
C(4)–C(5)	1.399(6)	1.396(5)	1.409(6)	1.391(6)	1.399(7)	1.418(4)
N(6)–C(5)	1.456(8)	1.430(4)	1.422(6)	1.428(6)	1.421(6)	1.432(3)
C(7)–C(8)	1.436(8)	1.425(5)	1.426(7)	1.421(7)	1.438(7)	1.431(4)
C(8)–C(9)	1.407(7)	1.413(5)	1.417(7)	1.405(7)	1.407(8)	1.417(4)
C(7)–H(7)	1.154(44)	0.96(4)	0.96(4)	0.92(5)	0.92(5)	0.96(3)
Bond angles (°)						
C–Sn(2)–C	124.1(3)	134.91(16)	141.2(3)	139.4(3)	132.7(4)	134.80(13)
O(1)–Sn(2)–O(3)	158.54(15)	156.23(9)	157.43(14)	156.89(14)	159.95(16)	156.43(8)
N(6)–Sn(2)–O(1)	85.4(2)	80.72(9)	81.89(14)	82.00(15)	83.46(17)	81.36(8)
N(6)–Sn(2)–O(3)	73.42(19)	76.57(10)	75.88(13)	76.02(14)	76.54(15)	75.80(8)
N(6)–Sn(2)–C	119.4(2)	116.35(13)	112.6(2)	114.4(2)	115.1(3)	116.18(11)
N(6)–Sn(2)–C	116.2(2)	107.95(13)	105.4(2)	106.0(2)	112.1(2)	108.88(11)
O(1)–Sn(2)–C	93.3(2)	86.90(14)	90.4(2)	88.0(2)	95.1(4)	89.34(12)
O(1)–Sn(2)–C	96.2(3)	92.37(15)	87.4(2)	93.4(2)	93.6(3)	94.04(12)
O(3)–Sn(2)–C	96.0(2)	101.19(15)	99.1(2)	99.4(2)	93.7(3)	98.73(12)
O(3)–Sn(2)–C	94.3(2)	96.87(14)	97.5(2)	94.5(2)	93.6(3)	95.49(13)
Sn(2)–O(1)–C(9)	129.0(3)	130.3(2)	134.6(3)	132.7(3)	134.3(4)	130.87(17)
Sn(2)–N(6)–C(5)	115.7(3)	111.6(2)	112.4(3)	111.9(3)	112.0(3)	112.90(18)
Sn(2)–N(6)–C(7)	125.8(6)	126.9(2)	127.1(3)	127.2(4)	126.5(4)	126.24(18)
Sn(2)–O(3)–C(4)	118.5(3)	116.5(2)	117.2(3)	117.2(3)	117.2(3)	116.87(18)
O(1)–C(9)–C(8)	122.9(4)	121.8(3)	123.0(4)	124.3(5)	123.0(5)	122.1(3)
C(4)–C(5)–N(6)	110.5(4)	114.9(3)	114.8(4)	114.7(4)	114.8(4)	114.0(2)
O(3)–C(4)–C(5)	120.2(4)	120.2(3)	119.8(4)	120.8(4)	120.3(5)	120.3(3)
C(7)–C(8)–C(9)	128.6(5)	124.1(3)	123.9(4)	123.7(4)	124.3(5)	123.5(3)
N(6)–C(7)–C(8)	123.5(6)	128.0(3)	128.7(5)	128.8(5)	127.5(5)	128.5(3)
Dihedral angles (°)						
Sn(2)–O(1)–C(9)–C(10)	165.0(4)	151.2(3)	179.4(4)	−173.1(5)	173.5(5)	152.6(2)
N(6)–C(7)–C(8)–C(13)	−177.9(5)	−168.9(3)	179.3(5)	179.1(5)	179.2(5)	−169.3(3)
Sn(2)–O(3)–C(4)–C(17)	167.3(4)	177.2(3)	178.9(4)	−177.5(4)	175.9(5)	176.7(2)
C(7)–N(6)–C(5)–C(14)	15.0(8)	9.9(5)	3.9(8)	−2.3(7)	9.0(8)	11.0(4)
Deviation from mean plane (Å)						
Plane: N(6)–C(5)–C(14)–C(15)–C(16)–C(17)–C(4)–O(3)						
Sn(2)	−0.335(5)	−0.096(3)	−0.024(4)	0.038(4)	0.185(7)	−0.120(3)
Plane: C(7)–C(8)–C(9)–C(10)–C(11)–C(12)–C(13)–O(1)						
Sn(2)	0.457(6)	0.773(4)	0.120(6)	−0.239(6)	−0.147(5)	0.742(3)
N(6)	−0.021(7)	0.234(4)	−0.102(6)	0.007(7)	0.005(4)	0.217(4)

than the distances found in TBP tin compounds (2.096 Å) [7,8,16,24]. The bond angles between both *alpha* carbons and the tin atom (C–Sn–C) are 124.1(3)° for **4a**, 134.91(16)° for **4b**, 141.2(3)°, 139.4(3)° and 132.7(4)° for the molecules present in **4d**, 134.80(13)° for compound **4e** (the average value in previously reported compounds is 126.99° for molecules that do not present O···Sn bridges or packing effects that modify the geometry of tin). The O(1)–Sn(2)–O(3) bond angle values are 158.54(15)° for **4a**, 156.23(9)° for **4b**, 157.43(14)°, 156.89(14)° and 159.95(16)° for **4d**, 156.43(8)° for **4e** being similar to those found in diorganotin^{IV} compounds possessing rigid tridentate ligands [31–36].

As a consequence of ring fusion, the O(3)–Sn(2)–N(6) bond angle in the five-membered ring shows values of 73.42(19)° for **4a**, 76.57(10)° for **4b**, 75.88(13)°, 76.02(14)° and 76.54(15)° for **4d**, 75.80(8)° for **4e** while the angles for the O(1)–Sn(2)–N(6)bonds are 85.4(2)° for **4a**, 80.72(9)° for **4b**, 81.89(14)°, 82.00(15)° and 83.46(17)° for **4d**, 81.36(8)° for compound **4e**.

2.5. Correlations between $\sigma_{Hammett}$ and NMR parameters

The Hammett equation is very useful for the study of intermolecular interactions, mainly of electronic type [37]. It is frequently used to determine the effect of aromatic substitution on reaction ratios for kinetic data, or the relative displacement of any chemical equilibrium for thermodynamic data. It has been used in electrochemical and kinetic techniques to elucidate reaction mechanisms.

As part of our investigation, the ^{15}N, ^{119}Sn (in $CDCl_3$ and DMSO-d_6) chemical shifts, as well as the $|^1J(^{119}Sn–^{13}C)|$ (Table 3) coupling constants of five *mono*-substituted di-*n*-butyltin^{IV} compounds (**4a**–**4b** and **4d**–**4f**) were correlated with $\sigma_{Hammett}$ values. Linear correlations were obtained with $\sigma_{Hammett}$ coefficients relative to O(3), using σ (*meta*) for **4a**, **4b**, **4d** and **4e** and σ (*para*) for **4f**. This indicates that the electronic effects are transmitted through the Sn(2)–O(3) bond and influence the acidity of the tin atom with linear modulation too.

The correlation of ^{15}N chemical shift vs. $\sigma_{Hammett}$ led to the equation, $\sigma_{Hammett} = -0.1054[\delta(^{15}N)] - 17.86$, where the correlation coefficient (R^2) has a value of 0.9848 (Fig. 3). The relationship between ^{15}N chemical shift and the $\sigma_{Hammett}$ shows that an electron donating substituent decreases the tin atom acidity and the nitrogen is weakly bonded to tin.

The ^{119}Sn chemical shift, in a non coordinating solvent ($CDCl_3$), vs. the $\sigma_{Hammett}$ gave the following equation, $\sigma_{Hammett} = 0.0881[\delta(^{119}Sn)] + 16.149$, (Fig. 4) with a correlation coefficient (R^2) of 0.9312. These results support the previous conclusions from ^{15}N NMR data, since electron-donation increases the density at the tin atom.

In the case of a coordinating solvent (DMSO-d_6), the opposite behaviour is observed, as shown in Fig. 5 ($\sigma_{Hammett} = -0.0326\ [\delta(^{119}Sn)] - 6.9579$, $R^2 = 0.9405$). The correlation between σ and ^{119}Sn chemical shifts denotes that an electron-withdrawing group increases the acidity of the tin atom and promotes coordination of the solvent in a stronger fashion. This clearly indicates that the presence of substituents in the aromatic ring serves as a modulator of O···Sn interactions. Even though the correlation factors in both ^{119}Sn NMR correlations ($CDCl_3$ and DMSO-d_6) are somewhat poor, the tendencies are useful to understand the molecular behaviour.

The plot of $|^1J(^{119}Sn–^{13}C)|$ coupling constants and $\sigma_{Hammett}$ (Fig. 6) gave the equation $\sigma_{Hammett} = -0.0783|^1J(^{119}Sn-^{13}C)| + 48.48$ with correlation coefficient (R^2) of 0.9753. The $|^1J(^{119}Sn–^{13}C)|$ coupling

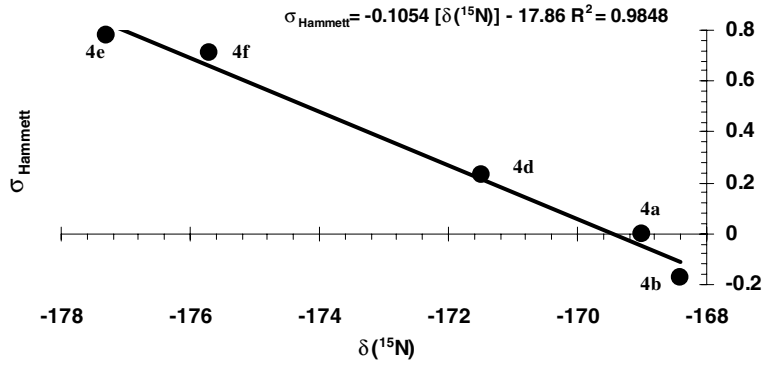

Fig. 3. Correlation between $\delta(^{15}N)$ and $\sigma_{Hammett}$.

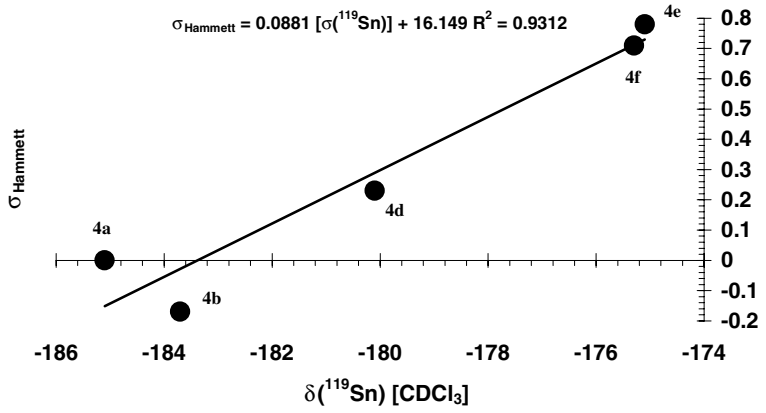

Fig. 4. Correlation between $\delta(^{119}Sn)$ in $CDCl_3$ and $\sigma_{Hammett}$.

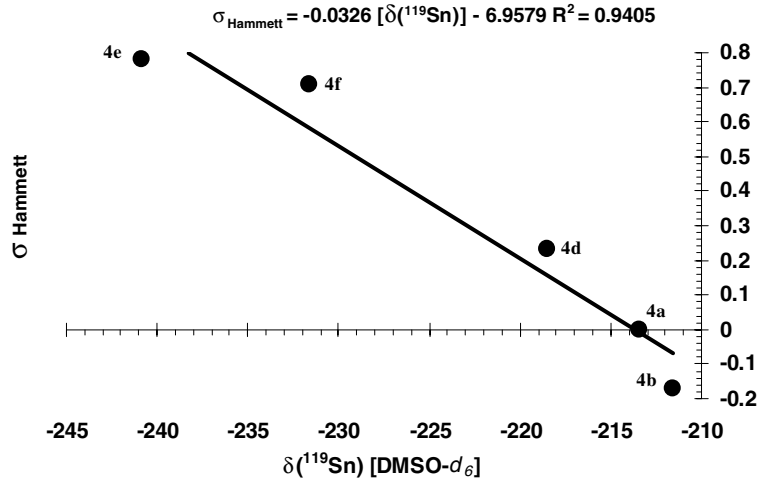

Fig. 5. Correlation between $\delta(^{119}\mathrm{Sn})$ in DMSO-d_6 and $\sigma_{\mathrm{Hammett}}$.

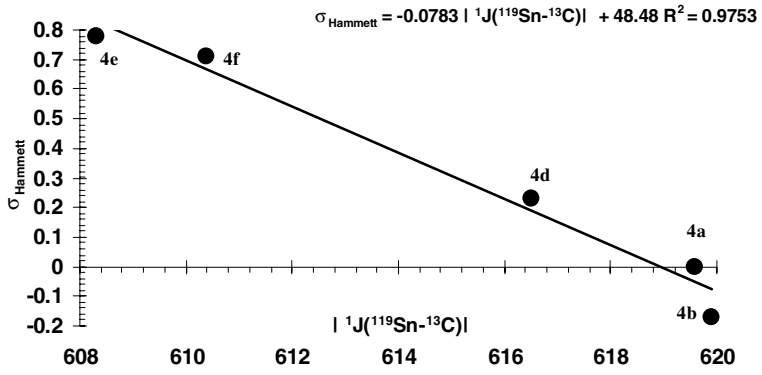

Fig. 6. Correlation between $|^{1}J(^{119}\mathrm{Sn}–^{13}\mathrm{C})|$in $CDCl_3$ and $\sigma_{\mathrm{Hammett}}$.

constant value is directly related to the C–Sn–C bond angle. Thus, an electron-releasing substituent increases this bond angle and thus the coupling constant. The C–Sn–C angle opening facilitates the formation of dimeric species with shorter Sn···O bridges, as seen in **4b** (3.0553(24) Å, Me substituent) while the opposite effect is evident in **4e** (3.2064(21) Å, NO_2 substituent).

3. Conclusions

An efficient one step procedure was used to prepare a series of 2,2-di-*n*-butyl-6-aza-1,3-dioxa-2-stanna-[d,h] dibenzocyclononenes (**4a**–**4f**) by in situ formation of a tridentate Schiff base ligand followed by addition of the di-*n*-butyltin^{IV} oxide to avoid isolation of the intermediate products.

The NMR data were conclusive to establish formation of the products based on the ^{15}N and ^{119}Sn chemical shift ranges that supported the N → Sn bond formation.

Compounds **4a** and one of the molecules in **4d** have a TBP tin atom while compounds **4b**, **4d** and **4e** crystallized within dimeric arrangements via the self-assembly of the tin atom with donor oxygen atoms, from the five-membered ring, to build a Sn_2O_2 four-membered ring moiety. In the dimeric structures, the tin atoms possess DOC geometry due to intermolecular O···Sn bridge formation. The specific case of compound **4d** consists of a cocrystal of two different molecules, one is monomeric and the other is dimeric, the former has a pentacoordinated tin atom and the latter has two hexacoordinated tin atoms. This crystal should be taken as an intermediate between the two possible crystalline phases.

The X-ray data for compounds **4a** and **4b** confirm the MAS-high power NMR data based on the ^{119}Sn spectra that show the pentacoordination of tin in **4a**, while it is hexacoordinated in **4b**.

The $\sigma_{\mathrm{Hammett}}$ and NMR data correlations provide important information concerning the N → Sn bond formation and stabilization, as well as electronic contributions related to C–Sn–C angle opening. The present correlations also provide guidelines to link molecules in supramolecular arrays taking advantage of stronger or weaker interactions that allow further building of interesting 2D or 3D architectures.

4. Experimental

All reagents and solvents were purchased as reagent grade quality and were used as received. Salicylaldehyde (**1**), di-*n*-butyltin oxide (**2**) and *ortho*-aminophenols (**3a-3f**) were purchased from Aldrich, benzene and ethanol were purchased from Fermont.

Solution NMR experiments were determined on a JEOL ECLIPSE-400 spectrometer at room temperature; chemical shifts (ppm) are relative to TMS and $SnMe_4$, coupling constants are quoted in Hz. The ^{119}Sn MAS-high power decoupling NMR spectra were acquired in a 4 mm CP-MAS probe at 111.92 MHz on a Bruker ASX-300 and referenced against neat $SnMe_4$. Mass spectra were obtained with a Hewlett–Packard 5994-A. Infrared spectra were recorded as KBr pellets on a Perkin–Elmer 16F PC FT-IR spectrophotometer. Melting points were measured in open capillary tubes on a Gallenkamp MFB 595 apparatus and are not corrected. Elemental analyses were obtained on an Eager 300 apparatus.

X-Ray single structure determinations were obtained on an Enraf Nonius-CAD4 ($\lambda_{Mo\ K\alpha} = 0.71073$ Å, graphite monochromator, $T = 293$ K, $\omega/2\theta$ scan mode) and an Enraf Nonius-FR590 Kappa-CCD ($\lambda_{Mo\ K\alpha} = 0.71073$ Å, graphite monochromator, $T = 293$ K, CCD rotating images scan mode). Crystals were glued in glass fiber sticks. When necessary, absorption correction was performed within the SHELX-A [38] program or by the semiempirical correction through MULTISCAN procedure (PLATON) [39]. All reflection data set were corrected for Lorentz and polarization effects. The first structure solution was obtained using the SHELX-S-97 program and then SHELX-L-97 ver. 34 program [38] was applied for refinement and output data. All software manipulations were done under the WIN-GX [40] environment program set. Molecular perspectives were drawn under ORTEP 3 [41] drawing application. All heavier atoms were found by Fourier maps difference and refined anisotropically. Some hydrogen atoms were found by Fourier maps differences and refined isotropically; the remaining hydrogen atoms were geometrically modeled and calculated for the refinement.

4.1. General procedure

Preparation of 2,2-di-*n*-butyl-6-aza-1,3-dioxa-2-stanna-[d,h]dibenzocyclononene (**4a**). To a previously dried flask were added 0.5 g (4.09 mmol) of salicylaldehyde (**1**), 0.447 g (4.09 mmol) of *ortho*-aminophenol (**2a**) and 1.02 g (4.09 mmol) of di-*n*-butyltin^{IV} oxide (**3**), to 100 mL of a 4:1 mixture of benzene and ethanol and the resulting saturated solution was maintained under reflux for eight hours. Compound **3** was not soluble under the reaction conditions but after 2 or 3 h, it reacts with the tridentate ligand formed in situ. After the reaction was completed, the crude product was evaporated under reduced pressure, the solid dissolved in 10 mL of dichloromethane and precipitated with hexane or petroleum ether to yield compound **4a** as a red powder.

All compounds were prepared using the same molar ratios described for **4a**.

4.2. 2,2-Di-n-butyl-6-aza-1,3-dioxa-2-stanna-[d,h]dibenzocyclononene (*4a*)

Red powder, yield 96%, 162–164 °C. ^{119}Sn MAS-high power decoupling NMR (111.92 MHz) $\delta = -185.8$. IR (ν) (KBr) 2950, 2918, 2850, 1606 (C=N), 1590 (C=N), 1536, 1478, 1466, 1438, 1394, 1320, 1300, 1282, 1270, 1148, 834, 744, 528 (Sn–O) cm^{-1}. MS *m/z* (%): 445 $M^+[^{120}Sn]$ (44), 443 $M^+[^{118}Sn]$ (34), 441 $M^+[^{116}Sn]$ (18), 388 $[^{120}Sn]$ (99), 386 $[^{118}Sn]$ (74), 384 $[^{116}Sn]$ (41), 330 $[^{120}Sn]$ (100), 328 $[^{118}Sn]$ (65), 326 $[^{116}Sn]$ (16). Elemental analysis, found: C, 56.84; H, 6.08; N, 3.18. Calculated for $C_{21}H_{27}NO_2Sn$: C, 56.79; H, 6.13; N, 3.15. Crystals suitable for X-ray diffraction analysis were obtained in a 4:1 mixture of hexane: dichloromethane.

4.3. 2,2-Di-n-butyl-6-aza-1,3-dioxa-15-methyl-2-stanna-[d,h]dibenzocyclononene (*4b*)

Red powder, yield 90%, 135–137 °C. ^{119}Sn MAS-high power decoupling NMR (111.92 MHz) $\delta = -220.2$. IR (ν) (KBr) 2958, 2920, 2852, 1604 (C=N), 1590 (C=N), 1538, 1492, 1472, 1440, 1386, 1322, 1290, 1268, 1254, 1154, 1128, 834, 764, 526 (Sn–O), 472 (Sn–N) cm^{-1}. MS *m/z* (%): 459 $M^+[^{120}Sn]$ (55), 457 $M^+[^{118}Sn]$ (39), 455 $M^+[^{116}Sn]$ (21), 402 $[^{120}Sn]$ (77), 400 $[^{118}Sn]$ (56), 398 $[^{116}Sn]$ (31), 345 $[^{120}Sn]$ (100), 343 $[^{118}Sn]$ (82), 341 $[^{116}Sn]$ (43). Elemental analysis, found: C, 57.49; H, 6.25, N, 3.10. Calculated for $C_{22}H_{29}NO_2Sn$: C, 57.67; H, 6.38; N, 3.06. Crystals suitable for X-ray diffraction analysis were obtained in a 7:2 ratio mixture of petroleum ether:dichloromethane.

4.4. 2,2-Di-n-butyl-6-aza-1,3-dioxa-15,17-dimethyl-2-stanna-[d,h]dibenzocyclononene (*4c*)

Red liquid, yield 82%, decomposes while heating. IR (ν) (KBr) 2956, 2920, 1606 (C=N), 1536, 1480, 1466, 1444, 1324, 1272, 1148, 522 (Sn–O), 470 (Sn–N) cm^{-1}. Elemental analysis, found: C, 58.32; H, 6.44, N, 3.16. Calculated for $C_{23}H_{31}NO_2Sn$: C, 58.50; H, 6.62; N, 2.97.

4.5. 2,2-Di-n-butyl-6-aza-1,3-dioxa-15-chloro-2-stanna-[d,h]dibenzocyclononene (*4d*)

Red powder, yield 86%, 84–85 °C. IR (ν) (KBr) 2958, 2918, 2852, 1606 (C=N), 1584 (C=N), 1532, 1476, 1464, 1438, 1386, 1288, 1276, 1210, 1148, 836, 526 (Sn–O), 474

(Sn–N) cm^{-1}. MS *m/z* (%): 479 $M^+[^{120}Sn]$ (40), 477 $M^+[^{118}Sn]$ (29), 475 $M^+[^{116}Sn]$ (13), 422 $[^{120}Sn]$ (75), 420 $[^{118}Sn]$ (54), 418 $[^{116}Sn]$ (26), 365 $[^{120}Sn]$ (100), 363 $[^{118}Sn]$ (73), 361 $[^{116}Sn]$ (31). Elemental analysis, found: C, 52.90; H, 5.55, N, 2.98. Calculated for $C_{21}H_{26}ClNO_2Sn$: C, 52.70; H, 5.48; N, 2.93. Crystals suitable for X-ray diffraction analysis were obtained in 8:1 hexane:dichloromethane mixture.

4.6. 2,2-Di-n-butyl-6-aza-1,3-dioxa-15-nitro-2-stanna-[d,h]dibenzocyclononene (*4e*)

Red powder, yield 74%, 99–101 °C. IR (*v*) (KBr) 2958, 2922, 2855, 1607 (C=N), 1538 (C=N), 1501, 1472, 1435, 1396, 1152, 840, 510 (Sn–O), 468 (Sn–N) cm^{-1}. MS *m/z* (%): 490 $M^+[^{120}Sn]$ (25), 488 $M^+[^{118}Sn]$ (19), 486 $M^+[^{116}Sn]$ (10), 433 $[^{120}Sn]$ (77), 431 $[^{118}Sn]$ (59), 429 $[^{116}Sn]$ (33), 377 $[^{120}Sn]$ (100), 375 $[^{118}Sn]$ (80), 373 $[^{116}Sn]$ (47). Elemental analysis, found: C, 51.84; H, 5.46, N, 6.15. Calculated for $C_{21}H_{26}N_2O_4Sn$: C, 51.57; H, 5.34; N, 6.02.

4.7. 2,2-Di-n-butyl-6-aza-1,3-dioxa-16-nitro-2-stanna-[d,h]dibenzocyclononene (*4f*)

Red solid, yield 78%, 78–80 °C. IR (*v*) (KBr) 2954, 2920, 2855, 1610 (C=N), 1515 (C=N), 1465, 1439, 1337, 1309, 1290, 1150, 561 (Sn–O), 471 (Sn–N) cm^{-1}. MS *m/z* (%): 490 $M^+[^{120}Sn]$ (21), 488 $M^+[^{118}Sn]$ (16), 486 $M^+[^{116}Sn]$ (9), 433 $[^{120}Sn]$ (73), 431 $[^{118}Sn]$ (53), 429 $[^{116}Sn]$ (29), 377 $[^{120}Sn]$ (100), 375 $[^{118}Sn]$ (82), 373 $[^{116}Sn]$ (49). Elemental analysis, found: C, 51.69; H, 5.25, N, 6.10. Calculated for $C_{21}H_{26}N_2O_4Sn$: C, 51.57; H, 5.34; N, 6.02.

5. Supplementary material

For compounds **4a**, **4b**, **4c** and **4e** full crystallographic data were submitted as CIF files with the Cambridge Crystallographic Data Center, CCDC Nos. 233165 for **4a**, 233166 for **4b**, 233167 for **4c** and 233168 for **4e**. CCDC, 12 Union Road, Cambridge CB21EZ, UK (fax: +44-1223-336033; e-mail: deposit@ccdc.cam.ac.uk or www: http://www.ccdc.cam.ac.uk).

Acknowledgement

The authors thank CONACyT for financial support and the scholarship to H.I. Beltrán during his Ph.D. Thanks are given to Consejo Superior de la Investigación Científica in Spain for the Cambridge Crystallographic Data Base license, to V. González for NMR spectra, D. Castillo for IR spectra and G. Cuellar for MS.

References

[1] J.M. Lehn, Supramolecular Chemistry: Concepts and Perspectives, VCH, Weinheim, 1995.
[2] G.R. Desiraju, Nature 412 (2001) 397.
[3] A. Jasat, J.C. Sherman, Chem. Rev. 99 (1999) 931.
[4] S. Mukamel, Nature 388 (1997) 425.
[5] R. van Heerbeek, P.C.J. Kamer, P. van Leeuwen, J.N.H. Reek, Chem. Rev. 102 (2002) 3717.
[6] D. Astruc, F. Chardac, Chem. Rev. 101 (2001) 2991.
[7] H.I. Beltran, L.S. Zamudio-Rivera, T. Mancilla, R. Santillan, N. Farfán, Chem. Eur. J. 9 (2003) 2291.
[8] R. García-Zarracino, J. Ramos-Quiñones, H. Höpfl, J. Organomet. Chem. 664 (2002) 188.
[9] R. García-Zarracino, J. Ramos-Quiñones, H. Höpfl, Inorg. Chem. 42 (2003) 3835.
[10] R. García-Zarracino, H. Höpfl, Angew. Chem., Int. Ed. 43 (2003) 1507.
[11] I. Haiduc, C. Silvestru, Organometallics in Cancer Chemotherapy, CRC Press, Boca Raton, FL, 1989;
M. Gielen, Appl. Organomet. Chem. 16 (2002) 481;
M. Nath, R. Yadav, M. Gielen, H. Dalil, D. de Vos, G. Eng. Appl. Organomet. Chem. 11 (1997) 727.
[12] S.J. Blunden, P.A. Cusack, R. Hill, Royal Society of Chemistry (Great Britain). The Industrial Uses of Tin Chemicals, Royal Society of Chemistry, London, 1985.
[13] F.H. Allen, Acta Cryst. B 58 (2002) 380. ;
I.J. Bruno, J.C. Cole, P.R. Edington, M. Kessler, C.F. Macrae, P. McCabe, J. Pearson, R. Taylor, Acta Cryst. B 58 (2002) 389;
I.J. Bruno, J.C. Cole, J.P.M. Lommerse, R.S. Rowland, R. Taylor, M. Verdonk, J Comput. Aided Mol. Des. 11-6 (1997) 525.
[14] S.P. Narula, S.K. Bharadwaj, Y. Sharda, R.O. Day, L. Howe, R.R. Holmes, Organometallics 11 (1992) 2206.
[15] D. Dakternieks, K. Jurkschat, S. van Dreumel, E.R.T. Tiekink, Inorg. Chem. 36 (1997) 2023.
[16] D. Dakternieks, T.S.B. Baul, S. Dutta, E.R.T. Tiekink, Organometallics 17 (1998) 3058.
[17] S.P. Narula, S. Kaur, R. Shankar, S. Verma, P. Venugopalan, S.K. Sharma, R.K. Chadha, Inorg. Chem. 38 (1999) 4777.
[18] S.P. Narula, S. Kaur, R. Shankar, S.K. Bharadwaj, R.K. Chadja, J. Organomet. Chem. 506 (1996) 181.
[19] M. Gielen, A. Bouhdid, R. Willem, V.I. Bregadze, L.V. Ermanson, E.R.T. Tiekink, J. Organomet. Chem. 501 (1995) 277.
[20] J. Beckmann, M. Biesemans, K. Hassler, K. Jurkschat, J.C. Martins, M. Schürmann, R. Willem, Inorg. Chem. 37 (1998) 4891.
[21] D. Kovala-Demertzi, N. Kourkoumelis, A. Koutsodimou, A. Moukarika, E. Horn, E.R.T. Tiekink, J. Organomet. Chem. 620 (2001) 194.
[22] V. Dokorou, Z. Ciunik, U. Russo, D. Kobala-Demertzi, J. Organomet. Chem. 630 (2001) 205.
[23] M. Gielen, Coord. Chem. Rev. 151 (1996) 41.
[24] S. Knoll, F. Tschwatschal, T. Gelbrich, T. Ristan, R.Z. Borsdorf, Z. Anorg. Allg. Chem. 624 (1998) 1015;
M. Tastekin, A. Kenar, O. Atakol, M.N. Tahir, D. Ülkü, Synth. React. Inorg. Met.-Org. Chem. 28 (1998) 10, 1727.
[25] M. Gielen, H. Dalil, L. Ghys, B. Boduszek, E.R.T. Tiekink, J.C. Martins, M. Biesemans, R. Willem, Organometallics 17 (1998) 4259.
[26] N.K. Goh, L.E. Khoo, T.C.W. Mak, Polyhedron 12 (1993) 925.
[27] H. Reyes, C. García, N. Farfán, R. Santillan, P.G. Lacroix, C. Lepetit, K. Nakatani, J. Organomet. Chem. 689 (2004) 2303.
[28] M. Nath, N. Chaudhary, Synth. React. Inorg. Met.-Org. Chem. 28 (1998) 121.
[29] L. Stefaniak, Ann. Rep. NMR Spectrosc. (1986) 18.

[30] A. Bondi, J. Phys. Chem. 68 (1964) 441.
[31] V.H. Pret, F. Huber, R. Barbieri, N. Bertazzi, Z. Anorg. Allg. Chem. 423 (1976) 75.
[32] A.J. Crowe, P.J. Smith, G. Atassi, Inorg. Chim. Acta 92 (1984) 100.
[33] G. Atassi, Rev. Si, Ge, Sn and Pb Comp. 8 (1985) 219.
[34] A. Meriem, R. Willem, J. Meunier-Piret, M. Gielen, M. Main Group Met. Chem. 8 (1989) 3.
[35] P.J. Sadler, Chem. Brit. 18 (1982) 182.
[36] Y. Arakawa, O. Wada, Suppression of Cell Proliferation by Certain Organotin Compounds, in: Proc. of the 2nd Symposium on Tin and Malignant Cell Growth, 1985, Ab.6, Scranton, PA.
[37] C.D. Johnson, The Hammett Equation, University Press, Cambridge, UK, 1973.
[38] G.M. Sheldrick, University of Göttingen, Göttingen, 1993.
[39] A.L. Spek, J. Appl. Crystallogr. 36 (2003) 7.
[40] L. Farrugia, J. Appl. Cryst. 32 (1999) 837.
[41] L. Farrugia, J. Appl. Cryst. 30 (1997) 565.